

Supporting Information

Tip-Enhanced Raman Spectromicroscopy of Co(II)-Tetraphenylporphyrin on Au(111): Toward the Chemists' Microscope

Joonhee Lee^{1†}, Nicholas Tallarida^{1†}, Xing Chen², Pengchong Liu², Lasse Jensen^{2*} and Vartkess Ara Apkarian^{1*}

1. Department of Chemistry, University of California, Irvine, Irvine, California, 92697, United States
2. Department of Chemistry, Pennsylvania State University, University Park, Pennsylvania 16802, United States

1. Optimized geometry

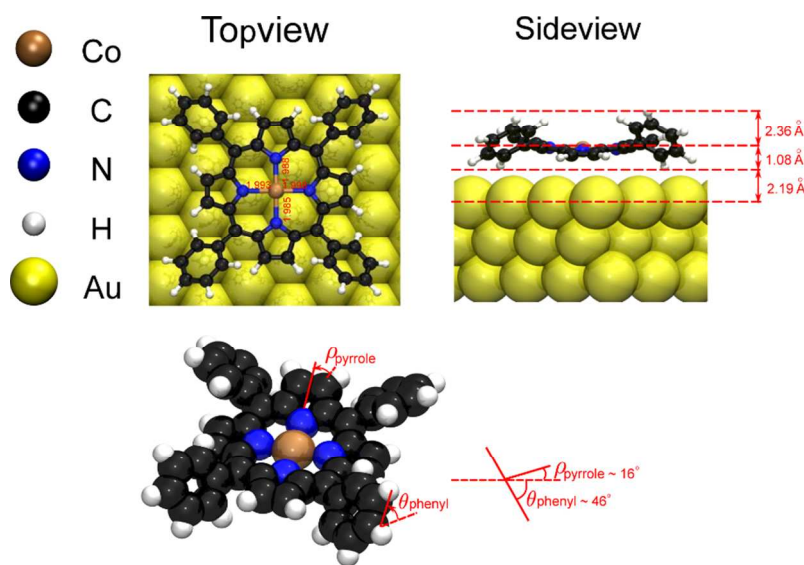


Figure S1. Optimized geometry of Co-TPP adsorbed on Au(111). The tilt angle of pyrrole moieties and rotation angle of the phenyl group are indicated at the bottom.

The geometry optimizations and frequency calculations of CoTPP adsorbed on the Au(111) surface and the free CoTPP were performed by the discrete interaction model-quantum mechanics (DIM/QM) method on ADF program package,^{1,2} at the spin-unrestricted BP86/DZP level of theory. The molecular force-field parameters needed from the DIM/QM were taken from the AMBER force field, and the parameters for Au atoms are $\sigma=1.7544$ kcal mol⁻¹ and $R=1.66$ Å. Only the image fields were included in the DIM/QM calculations. All molecular geometries and vibrations were rendered using the Visual Molecular Dynamics (VDM) 1.9.3 software.³

The saddled geometry of CoTPP on Au(111), calculated with the DIM/QM method,^{4,5} is shown in Figure S1. The phenyl groups twist to $\sim 46^\circ$, from 64° in the free molecule; and the twisted adjacent

phenyl groups tilt the diagonal pyrroles up and down away from the porphyrin macrocycle plane. The tilt angle of the pyrroles of 16° is smaller than the full DFT predicted value of 30° for CoTPP adsorbed on Ag(111), and the distance between Cobalt and Au (111) surface is 3.27 \AA , which is slightly longer than the calculated distance of 2.9 \AA between cobalt and Ag(111).⁶ These differences are likely to arise from the lack of charge transfer between molecule and surface in the present treatment, which is limited to van der Waals (VDW) and electrostatic interactions. The saddled molecule contains the necessary geometric features to scrutinize principles of vibrational spectromicroscopy with confined light.

2. Absorption spectrum

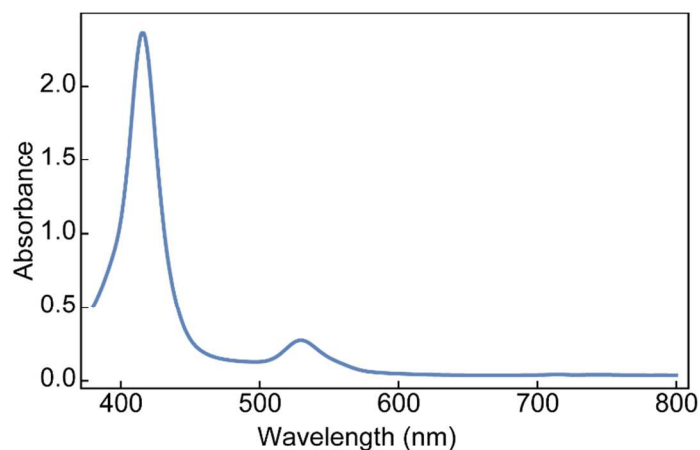


Figure S2. Absorption spectrum of CoTPP in toluene: The Q-band at 530 nm is far removed from the excitation wavelength at 634 nm.

3. Complete vibrational maps

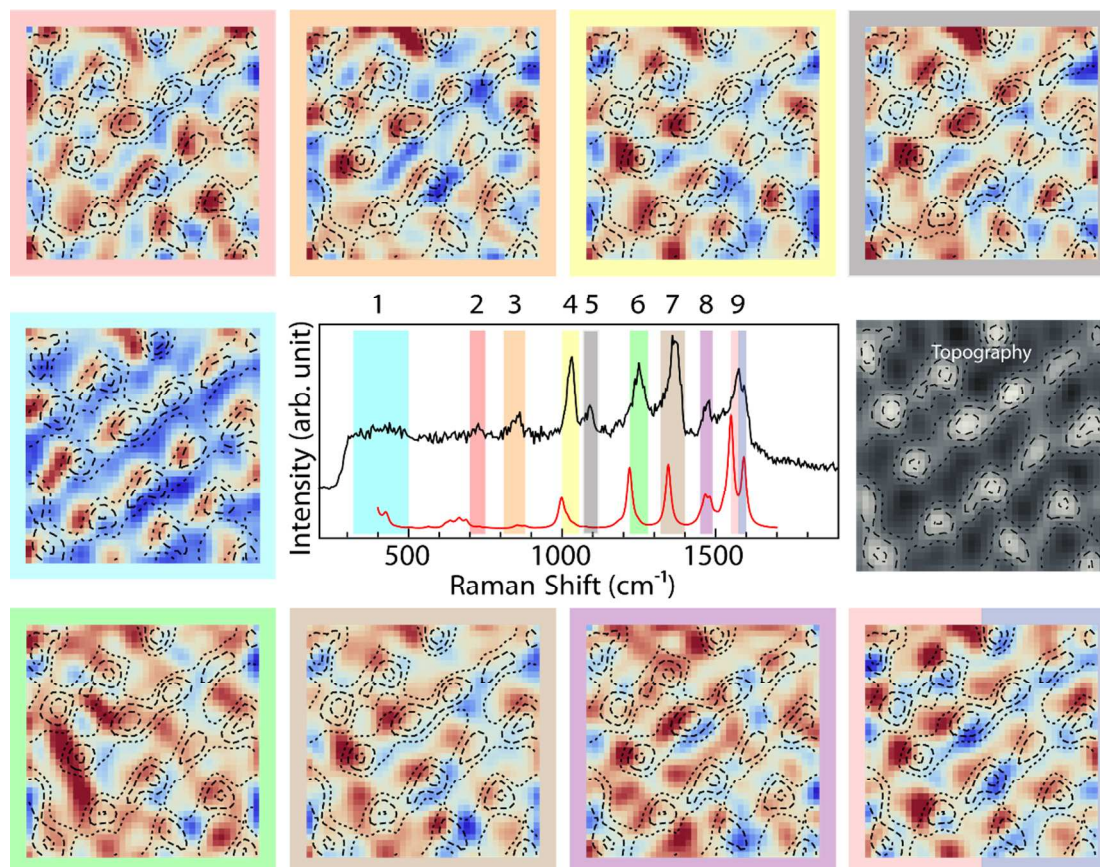


Figure S3. Fully decomposed vibrational maps. 9 vibrational maps are produced by subtracting the cavity-background and integrating individual vibrational peaks. Out of 9 mode-specific Raman images, mode 6 peaking at 1252 cm^{-1} is most anti-correlated with the topography represented by contours. The integration bands are: #1($320\text{-}500 \text{ cm}^{-1}$), #2($700\text{-}750 \text{ cm}^{-1}$), #3($810\text{-}880 \text{ cm}^{-1}$), #4($1000\text{-}1055 \text{ cm}^{-1}$), #5($1070\text{-}1110 \text{ cm}^{-1}$), #6($1220\text{-}1280 \text{ cm}^{-1}$), #7($1320\text{-}1400 \text{ cm}^{-1}$), #8($1450\text{-}1490 \text{ cm}^{-1}$), #9($1550\text{-}1600 \text{ cm}^{-1}$).

4. Raw images taken at room temperature

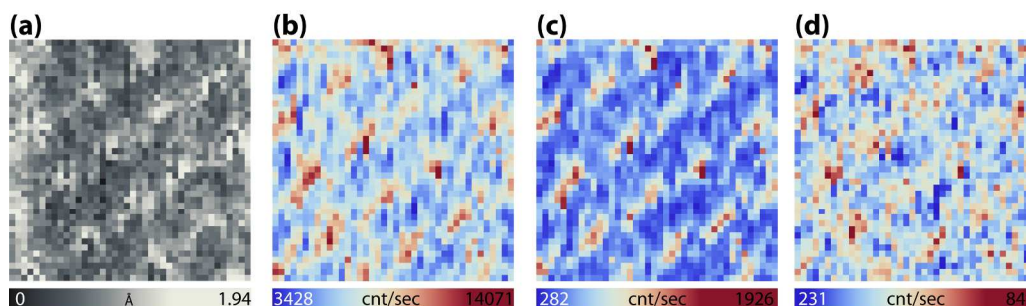


Figure S4. Raw image data obtained at room temperature. (a) STM topographic image taken at 10 pA and 0.15 V . ($57 \times 57 \text{ \AA}^2$) (b) Raman map integrated over the full vibrational window ($300\text{-}1700 \text{ cm}^{-1}$). (c) Cavity map integrated over a window ($320\text{-}500 \text{ cm}^{-1}$). (d) Map of mode #9 integrated over ($1550\text{-}1600 \text{ cm}^{-1}$).

5. Theoretical modeling of TERS junction

The TERS junction was modeled as an icosahedral Au₂₀₅₇ nanoparticle (tip) with an Au(111) surface as substrate. The substrate plane was the XY plane in the Cartesian system, and the tip retraction was along the Z axis. The Au₂₀₅₇ nanoparticle was constructed using FCC unit cells, and was placed on top of the substrate in a face-to-face conformation. Assuming the central Co atom of CoTPP molecule is at the Cartesian origin, the substrate plane is at Z=-2.5 Å. We use the Au-Au junction in the simulations to match the laser wavelength used in the experiment (532nm). The overall plasmonic response of the junction is determined mostly by the plasmonic response of the tip in our simulation. Therefore, we use an icosahedral nanoparticle consisting of 2057 atoms instead in the simulations to calculate the plasmon-induced near field. For the gold nanoparticle, the strongest and most confined near field is obtained at 2.32 eV (534nm).

Near field intensity, $I = |E|^2/|E_0|^2$, is calculated using an atomic electrodynamics model.^{5,7,8} In this work, the near field is polarized only in the Z direction. The frequent-dependent complex dielectric functions of metallic atoms were obtained from Johnson and Christy.⁹ The atomic polarizabilities of CO were fitted against results from linear response time-dependent density functional theory. The normalized field intensities in the Z direction were considered in the near-field distribution plots.

The near-field gradients were calculated by numerical differentiation between two nearest data points along each axis. The magnitude of the gradient was used in the field-gradient distribution plots, which was obtained from:

$$|\nabla E| = \sqrt{\left| \frac{E(x+\delta x)-E(x)}{\delta x} \right|^2 + \left| \frac{E(y+\delta y)-E(y)}{\delta y} \right|^2 + \left| \frac{E(z+\delta z)-E(z)}{\delta z} \right|^2}$$

The absolute values of the field and field gradients change with the gap distance, but the overall distribution patterns remain similar. The distribution plots in the main text were generated with the gap distance of about 9.5 Å (from the atomic center of the NP facet to the substrate surface, excluding the Au or CO tips).

The dependence of the near-field intensity on the gap distance was fitted into a linear model in a log-log scale. Here only the field intensity at the coordinate origin (also the position of the center Co atom) was sampled as the tip was retracted. Sampling at the origin is a reasonable approach to represent the field intensity-gap distance relation. It is a fixed position inside of the molecular geometry and it is on the line of the field maximum trajectory during the tip retraction.

6. Theoretical Simulation of TERS

The dressed tensor formalism¹⁰ in terms of the local fields, field gradients, and derivatives of electric dipole-dipole, electric dipole-quadrupole, and electric quadrupole-quadrupole polarizabilities was employed for the spectrum simulations. The local fields are created by a gold sphere with isotropic frequency-dependent polarizability. The polarizability, electric dipole, and electric quadrupole were obtained by the three-point numerical differentiation of the dipole moment and quadrupole moment. The magnitude of homogeneous external electric field was 5.14×10^8 V/m in the calculations. The derivatives of polarizabilities, dipole-quadrupole, and quadrupole-quadrupole tensors with respect to the mass-weighted normal modes were numerically calculated by three-point differentiation of the polarizabilities. The simulated Raman spectra were broadened by Lorentzians with full width at half

maxima of 20 cm^{-1} and 6.7 cm^{-1} for room temperature and low temperature, respectively, to be consistent with the experimental values.

Results and Discussions

The absorption spectrum of the junction has one prominent plasmonic peak at around 2.46 eV regardless of the gap size and tip type (icosahedral facet, CO molecule, and Au protrusion). The strongest and most confined near field is obtained at a slightly lower energy than the plasmonic resonance,⁷ which is 2.32 eV in this case. The confinement of the near field is necessary to generate strong field gradient.

For the bare tip, the near field is confined in the junction with the same shape as the icosahedral facet in the XY plane. The near field is evenly distributed within the junction. The field gradient is nearly zero, especially in the area around the sample molecule. The field gradient becomes stronger near the edges of the icosahedral facet, which is due to the confinement of the near field, but is unlikely to affect the molecular spectra. For the gap size of 9.5 \AA (tip facet $Z=7 \text{ \AA}$), the near-field maxima are at $Z_{\text{max}} = 2.4 \text{ \AA}$, which is well above the molecule.

When a single CO molecule is attached to the Au nanoparticle in the junction, the CO molecule serves as an atomically sharp tip and localizes the near field around it. The field localization brings about field gradient around the CO tip and changes the TERS spectrum of the CoTPP molecule. The field maxima are at $Z_{\text{max}} = 1.4 \text{ \AA}$, which overlaps with the molecular geometry. The height of the field maxima, or near-field focal plane, plays an important role in determining TERS spectra, especially for molecules with complex geometries.⁷ The overlapping of the focal plane and the molecular geometry is necessary to achieve high spatial resolution of TERS.

The field confinement effect becomes more significant when the atomic tip has higher polarizability. We replace the CO molecule with a single Au atom protrusion, and the near field in the junction is more confined, as evidenced by the increase both in the field maxima and field gradient maxima.

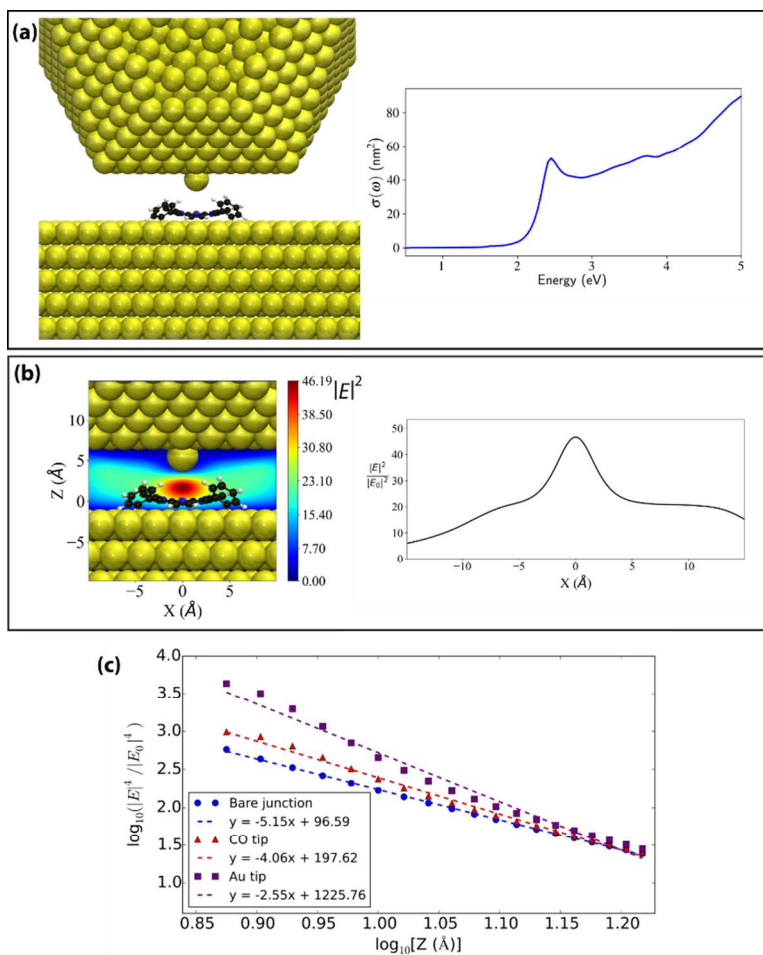


Figure S5. Theoretical modeling of TERS junction. (a) TERS junction with an atomically terminated tip with its plasmonic absorption spectrum. (b) Field distribution in the junction with a gold atom-terminated tip and a line profile cutting the highest intensity point. The FWHM is about 6 Å. (c) Gap dependence of field enhancement in the log-log plot.

7. Raw images acquired at 80 K

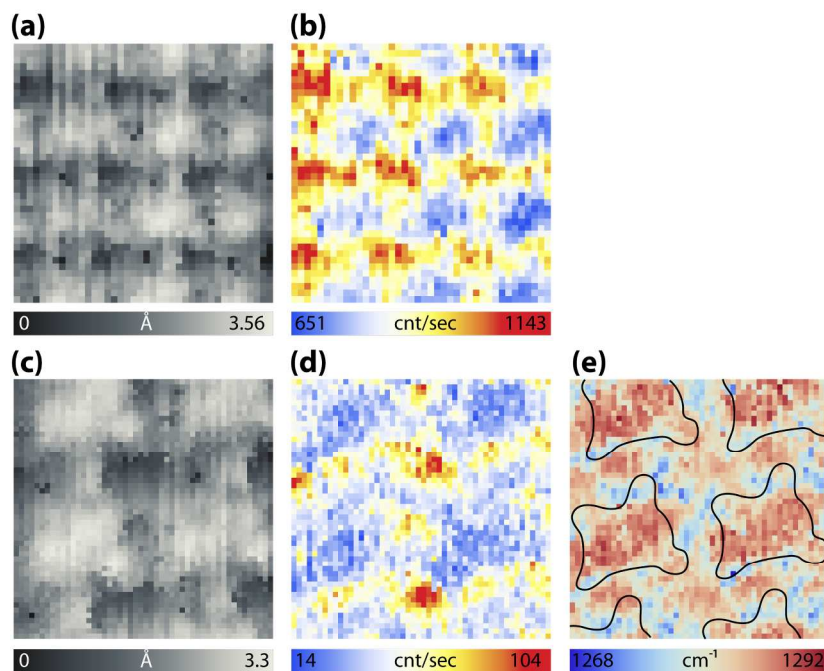


Figure S6. Raw images obtained at 80 K. (a) STM topographic image taken at 0.1 nA, 9.8 mV. (b) Simultaneously taken Raman map by integrating the intensity of 1270 cm^{-1} peak. (c) Magnified area inside (a), imaged at the same set point. (d-e) Super-resolution mapping. Amplitude (d) and frequency (e) map of Gaussian fit to 1270 cm^{-1} mode.

8. Field Gradients

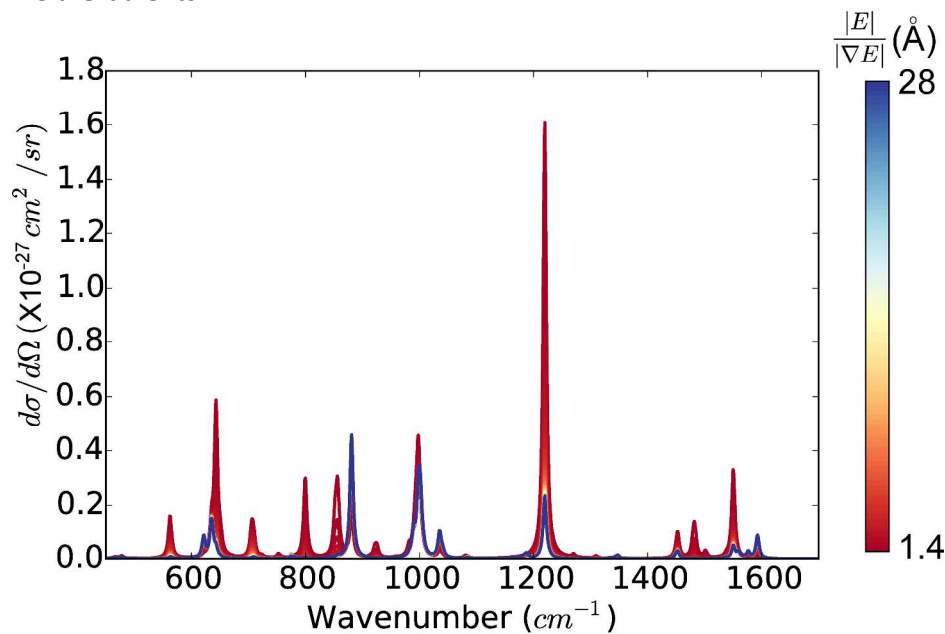


Figure S7. Simulated TERS of CoTPP in the flat geometry, excited with light polarized normal to the molecular plane. The effect of light confinement is modeled by varying the ratio of field-to-field gradient, shown in the color bar. The $E/\nabla E \sim 1.4\text{ \AA}$ is consistent with the degraded spectra seen at 80 K.

The vibrational modes activated by field gradient are color coded by red. We found when the ratio of field and field gradient is larger than 8 \AA , the spectral features do not change, which means the local field contribution is dominant. Evidently, the normal modes at 1220 cm^{-1} and at $700\text{-}900 \text{ cm}^{-1}$ are drastically enhanced by the large field gradient.

9. Multipolar expansion of Raman scattering tensors

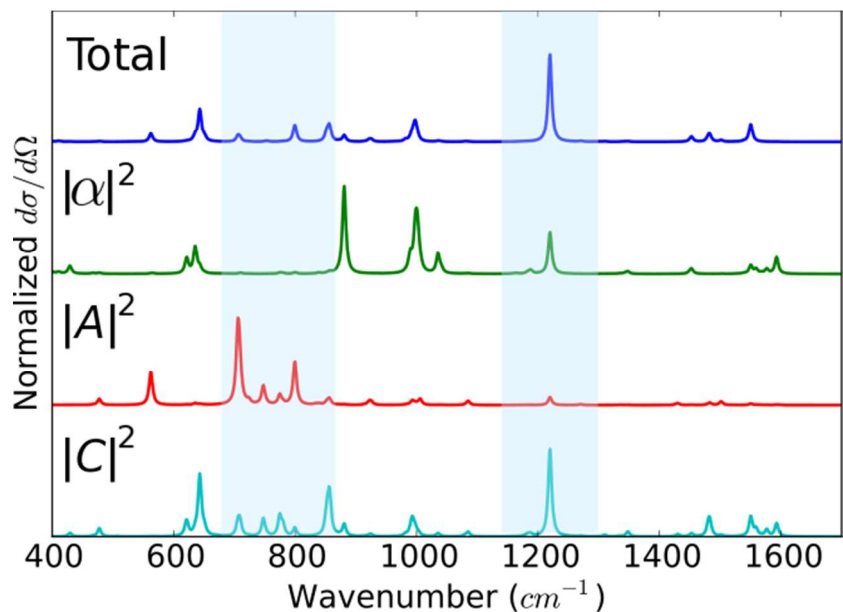


Figure S8. Multipolar Raman scattering components of the degraded spectrum used for Stark imaging. The three tensor components that are considered are the dipolar normal Raman, $|\alpha|^2$, field gradient driven dipole-quadrupole, $|A|^2$, and quadrupole-quadrupole, $|C|^2$, scattering terms. The latter dominates in the overall spectrum.

The further analysis of the polarizability contributions to the TERS under the large field gradient effects indicates the quadrupole-quadrupole polarizability plays a key role.

10. CO binding to CoTPP

Binding energy (BE) is defined as

$$BE = E_{\text{CoTPP}} + E_{\text{CO}} + E_{\text{CO}} - E_{\text{Bicarbonyl CoTPP}}$$

To isolate the binding energy, we subtract vdW interactions with Au surface from E_{CoTPP} and $E_{\text{Bicarbonyl CoTPP}}$ in the above equation.

Table S1. Binding energies of bicarbonyl CoTPP.

Bicarbonyl CoTPP	BE (eV)	BE without VDW (eV)	VDW (eV)
Axial	-0.77	0.27	1.04
Bridge	-0.34	-0.31	0.03

11. Predicted orientations of CoTPP and bicarbonyl CoTPP molecules at 80 K

The molecules originally lie on the xy plane, then reorientate by employing tilt angles for matching experimental spectra. The tilt angles are given in Table S1.

Table S2. Tilt angles in TERS simulations at 80 K

Molecule	Around x-axis (degree)	Around y-axis (degree)
CoTPP	5	10
Axial bicarbonyl CoTPP	20	15
Bridge bicarbonyl CoTPP	10	10

References

- (1) Baerends, E. J.; Autschbach, J.; Bashford, D.; Berces, A.; Bickelhaupt, F.; Bo, C.; Boerrigter, P.; Cavallo, L.; Chong, D.; Deng, L. . et al. Amsterdam Density Functional, 2016. [Http://www.scm.com](http://www.scm.com).
- (2) te Velde, G.; Bickelhaupt, F. M.; Baerends, E. J.; Fonseca Guerra, C.; van Gisbergen, S. J. A.; Snijders, J. G.; Ziegler, T. Chemistry with ADF. *J. Comput. Chem.* **2001**, *22*, 931–967.
- (3) Humphrey, W.; Dalke, A.; Schulten, K. VMD: Visual Molecular Dynamics. *J. Mol. Graph.* **1996**, *14*, 33–38.
- (4) Payton, J. L.; Morton, S. M.; Moore, J. E.; Jensen, L. A Discrete Interaction Model/quantum Mechanical Method for Simulating Surface-Enhanced Raman Spectroscopy. *J. Chem. Phys.* **2012**, *136*, 214103
- (5) Payton, J. L.; Morton, S. M.; Moore, J. E.; Jensen, L. A Hybrid Atomistic Electrostatics À Quantum Surface-Enhanced Raman Scattering. *Acc. Chem. Res.* **2013**, *47*, 88-91.
- (6) Auwärter, W.; Seufert, K.; Klappenberger, F.; Reichert, J.; Weber-Bargioni, A.; Verdini, A.; Cvetko, D.; Dell'Angela, M.; Floreano, L.; Cossaro, A.; et al. Site-Specific Electronic and Geometric Interface Structure of Co-Tetraphenyl-Porphyrin Layers on Ag(111). *Phys. Rev. B - Condens. Matter Mater. Phys.* **2010**, *81*, 1–14.
- (7) Liu, P.; Chulhai, D. V.; Jensen, L. Single-Molecule Imaging Using Atomistic Near-Field Tip-Enhanced Raman Spectroscopy. *ACS Nano* **2017**, *11*, 5094–5102.
- (8) Chen, X.; Moore, J. E.; Zekarias, M.; Jensen, L. Atomistic Electrostatics Simulations of Bare and Ligand-Coated Nanoparticles in the Quantum Size Regime. *Nat. Commun.* **2015**, *6*, 8921.
- (9) Johnson, P. B.; Christy, R. W. Optical Constants of the Noble Metals. *Phys. Rev. B* **1972**, *6*, 4370–4379.
- (10) Chulhai, D. V.; Jensen, L. Determining Molecular Orientation With Surface-Enhanced Raman Scattering Using Inhomogeneous Electric Fields. *J. Phys. Chem. C* **2013**, *117*, 19622–19631.